Torque Limit-based Inertial Control Method Based on Delayed Support for Primary Frequency Control of Wind Turbines

Wei Gu, Zaiyu Chen, Qun Li, Minghui Yin, Qiang Li, and Yun Zou

***Abstract*—To avoid the secondary frequency dip caused by the steep drop of the electrical power of wind turbines (WTs) at the end of frequency support stage, the torque limit-based inertial control (TLIC) method sets the power reference as a linear function of rotor speed, rather than the step form for the stepwise inertial control. However, the compensation effect on the frequency nadir (FN) caused by the load surge is weakened as the TLIC power is no longer in the step form. Specifically, the maximum point of the frequency response component (FRC) contributed by TLIC occurs earlier than the minimum point of FRC corresponding to the load surge, so that the FN cannot be adequately raised. Therefore, this paper first investigates the relation between the peak and nadir times of FRCs stimulated by the TLIC and load power. On this basis, with the compensation principle of matching the peak and nadir times of FRCs, the improved TLIC method based on delayed support is proposed. Finally, the effectiveness of the proposed method is validated via the experiments on the test bench of wind-integrated power system.**

***Index Terms*—Wind turbine, frequency response component, torque limit, inertial control, delayed support.**

I. Introduction

With the deepening increase in wind power penetration, the inertia of the power system significantly decreases. Wind turbines (WTs) are urgently required to participate in the primary frequency control (PFC) [1]-[5]. According to whether the electrical power of WTs is related to the frequency, the existing PFCs can be divided into two types: PFC strategies responding to the frequency variation such as virtual inertial control [6], [7] and droop control [7], and PFC strategies presetting the power curves such as stepwise inertial control (SIC) [8]-[11] and torque limit-based inertial control (TLIC) [12]-[14]. This paper mainly focuses on the second type.

The PFC strategies with preset power curves generally consist of two stages: frequency support and rotor speed recovery. When the load increases suddenly in the power system, the SIC method increases the electrical power of WTs by the step form to support the active power balance [8]-[11]. From the perspective of the frequency response component (FRC) superposition and compensation [9], the SIC is eminently suitable for compensating the load surge during the frequency support stage. Due to the identical step forms, the FRCs, excited by SIC power and load surge, respectively, reach the peak and the nadir simultaneously. Particularly, if the electrical power increment of WTs is the same as the load increment, the frequency variation caused by the load surge can be fully compensated by the FRC of SIC power, and the frequency is able to be kept at the rated value.

Due to the limited kinetic energy, it is known that the steep reduction in SIC power at the end of the frequency support stage leads to the secondary frequency dip (SFD) [11], [12]. Hence, how to coordinate the PFCs of WTs and synchronous generators (SGs) to mitigate the SFD has become one of the focuses in the existing research. The main developments are summarized in the following two aspects.

1) SIC-based improvements, including smoothing the exit curve [15] and setting the termination time [9]-[11]. It is worth noting that [9] proposed the fixed termination time (FTT) of SIC. Based on the analysis of the FRC superposition and compensation under different power stimuli, the principle of determining FTT is that the nadir of the FRC for the step reduction of the SIC power occurs simultaneously with the peak of that for the load surge. This FRC compensation strategy not only alleviates the SFD effectively, but also presents a novel approach to the coordination between WTs and SGs, e.g., terminating the PFC strategies when the output power of SGs is sufficiently promoted.

2) Improved methods with the characteristic of gradual power drop [12]-[14], [16]-[18]. Considering that the steep power drop is the root cause of SFD, the improved methods were proposed so that the electrical power of WTs varies along with the rotor speed, e.g., TLIC [12], [14]. Since the

Manuscript received: November 25, 2022; revised: February 24, 2023; accepted: April 17, 2023. Date of CrossCheck: April 17, 2023. Date of online publication: June 14, 2023.

This work was supported by the National Natural Science Foundation of China (No. 51977111), the "Six Talent Peaks" High-level Talent Project in Jiangsu Province (No. XNY-025), the Special Fund of Jiangsu Province for Transformation of Scientific and Technological Achievements (No. BA2019045), and the Jiangsu Qinglan Project.

W. Gu, Z. Chen (corresponding author), M. Yin, and Y. Zou are with the School of Automation, Nanjing University of Science and Technology, Nanjing 210094, China (e-mail: dafenguwei@126. com; zaiyu. chen@njust. edu. cn; ymhui@vip.163.com; zouyun@vip.163.com).

Q. Li and Q. Li are with the State Grid Jiangsu Electric Power Co., Ltd. Research Institute, Nanjing 211103, China (e-mail: qun_li@sina.com; 35830342@qq.com).

DOI: 10.35833/MPCE.2022.000773

rotor speed decreases gradually with the release of kinetic energy, the electrical power of WTs in the frequency support stage decreases slowly, thus avoiding the impact of the exit of WTs on the active power balance.

However, the TLIC in non-step form of electrical power of WTs diminishes the effectiveness of compensating the frequency nadir (FN) caused by load surge. In this paper, it is found that the maximum point of the FRC excited by the TLIC power occurs earlier than the minimum point of the FRC excited by the load surge. That is, the maximum effect of WTs for frequency support appears too early to sufficiently compensate the FN. In this regard, this paper firstly derives the expression of the FRC corresponding to the TLIC method, and then investigates the relationship between its maximum point and minimum point of the FRC. On this basis, the improved TLIC method based on delayed support is proposed. Based on the estimation of the delay time, the proposed method delays triggering the TLIC method, so the FRC compensation by matching the peak and nadir times is realized. This paper also presents a mechanism explanation for the discovery of the improved frequency regulation performance with the delayed support from WTs [19]. Finally, the effectiveness of the proposed method is validated via the experiments on the test bench of wind-integrated power system.

The key contributions of this paper can be summarized as follows.

1) It is found that the maximum point of the FRC excited by the PFCs of WTs does not always occur at the FN caused by the load surge, which makes the maximum compensation effect for the FN not sufficient. Thus, the PFC performance of WTs is limited.

2) From the perspective of the FRC superposition and compensation, it is analyzed and found that the maximum point of the FRC excited by the TLIC power occurs earlier. Hence, the improved idea that the extreme point time is matched is proposed, so that the maximum effect of the TLIC power is exerted at the FN caused by the load surge.

3) The improved TLIC method based on the delayed support is proposed, in which the optimal delay time can be calculated quantitatively. By delaying the start of the TLIC method, the FN can be further enhanced without destabilizing the WT.

The remainder of this paper is organized as follows. Section II introduces the WT model and the PFC. Section III analyzes the frequency regulation effect of the TLIC method from the perspective of the FRC compensation. In Section IV, the improved TLIC method based on delayed support is proposed. The effectiveness of the proposed method is validated by experiments in Section V. Finally, conclusions are drawn in Section VI.

II. WT Model and PFC

Different from virtual inertial control and droop control responding to the frequency variation, the PFCs proposed in [8]-[14] preset the power curves. When the frequency event (e.g., the load increase) occurs in the grid, the electrical power of WTs is set according to the curve which is irrelevant to the frequency variation, such as the curve obtained by SIC [8]-[11] and TLIC [12]-[14].

A. Modeling of WTs

The block diagram of the variable-speed WT is shown in Fig. 1, where RSC stands for rotor-side converter; and GSC stands for grid-side converter. The RSC controls the generator output power, and the GSC maintains the stability of the direct-current voltage [20]. Considering that the electromagnetic dynamics are much faster than the mechanical dynamics [21], this paper focuses on the latter, which is on the same time scale as the frequency variation f, and assumes that the generator control can respond to the torque reference $T_{g,ref}$ quickly and precisely.

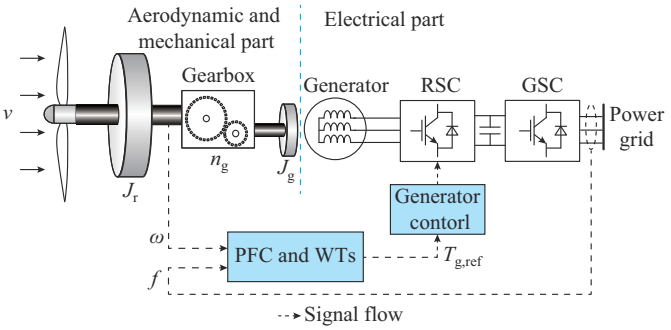

Fig. 1. Block diagram of variable-speed WT.

The aerodynamic power P_m captured by the rotor from the wind is described as:

$$P_m = \frac{1}{2}\rho\pi R^2 v^3 C_p(\lambda,\beta) \tag{1}$$

$$\lambda = \frac{\omega R}{v} \tag{2}$$

where ρ, R, and v are the air density, rotor radius, and wind speed, respectively; C_p is the power coefficient, which is a nonlinear function of the tip speed ratio (TSR) λ and the pitch angle β, and a common aerodynamic characteristic [22], [23] is shown by (3); and ω is the rotor speed. The maximum power coefficient C_{pmax} is obtained at the optimal TSR λ_{opt} when the pitch angle is 0°.

$$\begin{cases} C_p(\lambda,\beta) = 0.5176\left(\dfrac{116}{\lambda_i} - 0.4\beta - 5\right)e^{-\frac{21}{\lambda_i}} + 0.0068\lambda \\ \dfrac{1}{\lambda_i} = \dfrac{1}{\lambda + 0.08\beta} - \dfrac{0.035}{\beta^3 + 1} \end{cases} \tag{3}$$

The mechanical dynamics of the WT mainly refer to the speed change of the drive-train consisting of a rotor and a generator. When the gear ratio of the gearbox is n_g, the mechanical dynamics can be represented by a two-mass model [21] as:

$$\begin{cases} J_r\dot{\omega} = T_m - D_r\omega - T_{ls} \\ J_g\dot{\omega}_g = T_{hs} - D_g\omega_g - T_g \\ n_g = \omega_g/\omega = T_{ls}/T_{hs} \end{cases} \tag{4}$$

where J_r and J_g are the inertia values of the rotor and generator, respectively; ω_g is the generator speed; T_{ls} and T_{hs} are the low-speed and high-speed shaft torques, respectively; D_r

and D_g are the damping factors of the rotor and generator, respectively; and T_m and T_g are the aerodynamic and electromagnetic torques, respectively.

If the damping factors of the rotor and generator are ignored, the single-mass model [24] is derived as:

$$J_t\dot{\omega}=T_m-T_e=\left(P_m-P_e\right)/\omega \tag{5}$$

where $J_t=J_r+n_g^2J_g$ is the total inertia equivalent to the low-speed shaft; $T_e=n_gT_g$ is the generator torque equivalent to the low-speed shaft; and P_e is the output power.

Normally, the WT operates in the maximum power point tracking (MPPT) mode, and the power command P_{MPPT} is

$$P_{MPPT}=K_{opt}\omega^3 \tag{6}$$

where $K_{opt}=0.5\rho\pi R^5C_{Pmax}/\lambda_{opt}^3$ is the optimal power curve coefficient.

B. TLIC Method

For the SIC method, the WT over-produces the constant electrical power for a period of time [8], [25], and then reduces the power to restore the rotor speed. The sudden power drop easily causes the SFD, which can even be worse than the condition without the power support provided by the WT. To address this problem, the TLIC method was proposed in [12], [14]. The linear relationship is established between the TLIC power and the rotor speed, so the power decreases gently with the decrease of rotor speed, thus avoiding the large and sudden power drop.

As shown in Fig. 2, when a load surge event occurs, the TLIC method immediately increases the electrical power from P_{W0} to $P_{T_{lim}}(\omega_0)$, and sets the power $P_{TLIC}(\omega)$ according to the rotor speed during the frequency support stage (B-C), as shown in (7). The WT operates along the preset power-speed curve.

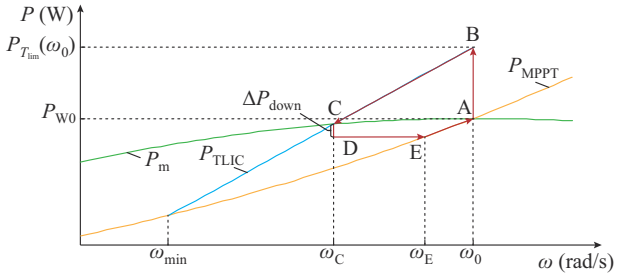

Fig. 2. Illustration of TLIC method.

$$P_{TLIC}(\omega)=K_{P\text{-}\omega}\left(\omega-\omega_0\right)+P_{T_{lim}}(\omega_0) \tag{7}$$

$$K_{P\text{-}\omega}=\frac{P_{T_{lim}}(\omega_0)-P_{MPPT}(\omega_{min})}{\omega_0-\omega_{min}} \tag{8}$$

where $K_{P\text{-}\omega}$ is the slope of the power-speed curve; $P_{T_{lim}}(\omega_0)$ is the power corresponding to the torque limit T_{lim} at the initial rotor speed ω_0 $\left(P_{T_{lim}}(\omega_0)=T_{lim}\omega_0\right)$; ω_{min} is the minimum rotor speed; and $P_{MPPT}(\omega_{min})$ is the optimal power corresponding to ω_{min}.

During the frequency support stage, the electrical power is always higher than the aerodynamic power (the green line) and the WT decelerates. Besides, the electrical power decreases with the decrease of rotor speed. When the rotor speed decreases to the speed ω_C corresponding to the intersection point C, the electrical power is equal to the aerodynamic power and the WT operates at the stable equilibrium point. Then, the rotor is accelerated to ω_0 along the D-E-A curve. The electrical power is reduced to a constant value P_{rec} by a small reduction ΔP_{down}. Until the WT accelerates to point E, namely $\omega>\omega_E$, the electrical power is set according to (6) (the yellow line).

$$P_{rec}=P_{TLIC}(\omega_C)-\Delta P_{down} \tag{9}$$

$$\omega_E=\sqrt[3]{\frac{P_{rec}}{K_{opt}}} \tag{10}$$

The solid red line in Fig. 2 shows the complete trajectory of the TLIC method. Obviously, the electrical power of WTs is no longer in the same step form as the load surge. It is noted that the slight drop of electrical power has a small impact on the frequency, so this paper mainly focuses on the frequency support stage.

III. Analysis of Frequency Regulation Effect of TLIC Method Based on FRC Compensation

As shown in Fig. 3, the load disturbance ΔP_L and the electrical power deviation of WTs ΔP_W are considered as the input signals of the system frequency response model [26]. $G(s)$ is the system frequency response model; ΔP_M is the mechanical power increment of the synchronous generator; H is the inertia constant of the equivalent system; D is the damping factor; R_g is the governor regulation factor; K_m is the mechanical power gain factor; F_H is the fraction of total power generated by the high pressure turbine; T_R is the reheat time constant; and Δf is the frequency deviation. According to the superposition principle of linear systems [27], FRCs of the load disturbance and the electrical power deviation of WTs are analyzed, respectively, and then the comprehensive effect on the frequency can be obtained. Therefore, this section analyzes the effects of the TLIC method on improving the FN from the perspective of the mutual compensation of the two FRCs.

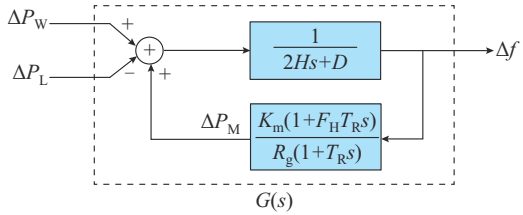

Fig. 3. System frequency response model.

A. FRC of TLIC Power

When the WT operates in the MPPT mode, the system frequency response only under the load power is

$$\Delta f_L(t)=L^{-1}\left(\Delta f_L(s)\right)=L^{-1}\left(G(s)\Delta P_L(s)\right) \tag{11}$$

where $L^{-1}(\cdot)$ is the inverse Laplace transform. Meanwhile, the system frequency response only under the wind power is

$$\Delta f_W(t)=L^{-1}\left(\Delta f_W(s)\right)=L^{-1}\left(G(s)\Delta P_W(s)\right) \tag{12}$$

Hence, when the WT is involved in the PFC to deal with the load disturbance, the actual frequency response is the superposition of (11) and (12), as shown in Fig. 4.

$$\Delta f(t)=\Delta f_{\mathrm{L}}(t)+\Delta f_{\mathrm{W}}(t) \tag{13}$$

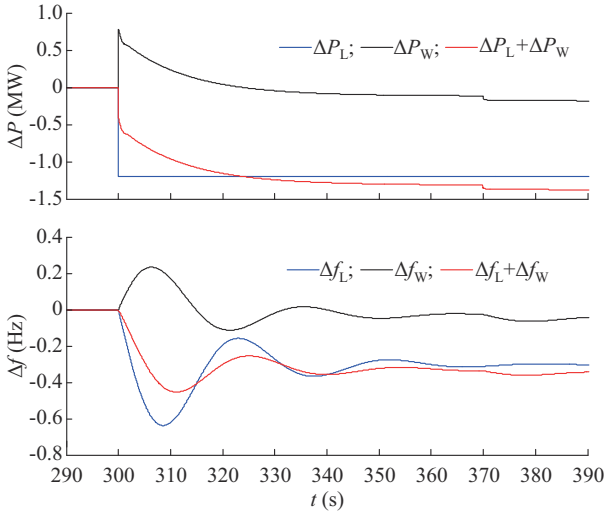

Fig. 4. FRCs.

For the load surge event, (11) is specified as the frequency response excited by the step power:

$$\Delta f_{\mathrm{L}}(t)=\Delta P_{\mathrm{L}} h_{\mathrm{step}}(t) \tag{14}$$

where $h_{\mathrm{step}}(t)$ is the unit step response of $G(s)$ [26].

$$h_{\mathrm{step}}(t)=r\left(1+\alpha \mathrm{e}^{-\xi\Omega_{\mathrm{n}}t}\sin\left(\Omega_{\mathrm{r}}t+\phi\right)\right) \tag{15}$$

$$\begin{cases} r=\dfrac{R_{\mathrm{g}}}{DR_{\mathrm{g}}+K_{\mathrm{m}}} \\ \Omega_{\mathrm{n}}=\sqrt{\dfrac{DR_{\mathrm{g}}+K_{\mathrm{m}}}{2HR_{\mathrm{g}}T_{\mathrm{R}}}} \\ \xi=\dfrac{2HR_{\mathrm{g}}+\left(DR_{\mathrm{g}}+K_{\mathrm{m}}F_{\mathrm{H}}\right)T_{\mathrm{R}}}{2\left(DR_{\mathrm{g}}+K_{\mathrm{m}}\right)}\Omega_{\mathrm{n}} \\ \Omega_{\mathrm{r}}=\Omega_{\mathrm{n}}\sqrt{1-\xi^2} \\ \alpha=\sqrt{\dfrac{1-2\xi T_{\mathrm{R}}\Omega_{\mathrm{n}}+T_{\mathrm{R}}^2\Omega_{\mathrm{n}}^2}{1-\xi^2}} \\ \phi=\arctan\left(\dfrac{\Omega_{\mathrm{r}}T_{\mathrm{R}}}{1-\xi\Omega_{\mathrm{n}}T_{\mathrm{R}}}\right)-\arctan\left(\dfrac{\sqrt{1-\xi^2}}{-\xi}\right) \end{cases} \tag{16}$$

Since the form of the TLIC power is a complex and nonlinear function of time, the power is simplified as the segmented function in Fig. 5 [9].

$$\Delta P_{\mathrm{W}}(t)=\Delta P_{\mathrm{W0}}u\left(t-t_0\right)+\sum_{i=1}^{N}\left(K_{P\text{-}t}^{i}\left(t-t_{i-1}\right)u\left(t-t_{i-1}\right)-K_{P\text{-}t}^{i}\left(t-t_i\right)u\left(t-t_i\right)\right) \tag{17}$$

where ΔP_{W0} is the initial power increment, $\Delta P_{\mathrm{W0}}=P_{T_{\mathrm{lim}}}(\omega_0)-P_{\mathrm{W0}}$; $K_{P\text{-}t}^{i}$ is the slope of the i^{th} segment; $u(t)$ is the unit step signal; and N is the number of the segments.

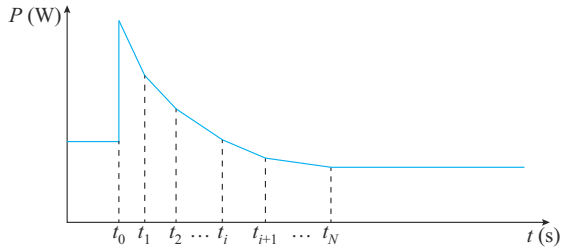

Fig. 5. Segmented function of TLIC power.

On this basis, the frequency response under the simplified TLIC power is shown in (18), which is expressed as a superposition of the frequency responses of a step signal and multi-ramp signals.

$$\Delta f_{\mathrm{W}}(t)=\Delta P_{\mathrm{W0}}h_{\mathrm{step}}\left(t-t_0\right)u\left(t-t_0\right)+\sum_{i=1}^{N}\left(K_{P\text{-}t}^{i}h_{\mathrm{ramp}}\left(t-t_{i-1}\right)u\left(t-t_{i-1}\right)-K_{P\text{-}t}^{i}h_{\mathrm{ramp}}\left(t-t_i\right)u\left(t-t_i\right)\right) \tag{18}$$

where $h_{\mathrm{ramp}}(t)$ is the unit slope response of $G(s)$ [9].

$$h_{\mathrm{ramp}}(t)=rt-\frac{r\alpha}{\xi^2\Omega_{\mathrm{n}}^2+\Omega_{\mathrm{r}}^2}\mathrm{e}^{-\xi\Omega_{\mathrm{n}}t}\left(\xi\Omega_{\mathrm{n}}\sin\left(\Omega_{\mathrm{r}}t+\phi\right)+\Omega_{\mathrm{r}}\cos\left(\Omega_{\mathrm{r}}t+\phi\right)\right)+\frac{r\alpha}{\xi^2\Omega_{\mathrm{n}}^2+\Omega_{\mathrm{r}}^2}\left(\xi\Omega_{\mathrm{n}}\sin\phi+\Omega_{\mathrm{r}}\cos\phi\right) \tag{19}$$

B. Comparison of Extreme Point Time of $\Delta f_{\mathrm{W}}(t)$ and $\Delta f_{\mathrm{L}}(t)$

Reference [26] pointed out that the nadir time under the step power excitation is fixed, which is only related to the system parameters and irrelevant to the step amplitude. Considering that the SIC power and load surge are in the same step form, it takes the same time to reach the maximum/minimum points of the FRC (denoted as $\Delta t_{\mathrm{L}}^{\mathrm{nadir}}$), so the SIC power can achieve the best compensation effect on the FN. And the minimum point time is $t_{\mathrm{L}}^{\mathrm{nadir}}$.

$$\Delta t_{\mathrm{L}}^{\mathrm{nadir}}=\frac{1}{\Omega_{\mathrm{r}}}\arctan\left(\frac{\Omega_{\mathrm{r}}T}{\xi\Omega_{\mathrm{n}}T-1}\right) \tag{20}$$

However, the TLIC power shown in (16) is no longer in the step form, so the frequency response and the maximum point time change, which consequently affects the frequency regulation effect of WTs. Taking the derivative of (18), the change rate of the frequency corresponding to the TLIC power is

$$\Delta f_{\mathrm{W}}'(t)=\begin{cases} \Delta P_{\mathrm{W0}}h_{\mathrm{step}}'\left(t-t_0\right)+\sum_{j=1}^{i-1}\left(K_{P\text{-}t}^{j}h_{\mathrm{ramp}}'\left(t-t_{j-1}\right)-K_{P\text{-}t}^{j}h_{\mathrm{ramp}}'\left(t-t_j\right)\right)+ \\ \quad K_{P\text{-}t}^{i}h_{\mathrm{ramp}}'\left(t-t_{i-1}\right) \quad t_{i-1}<t\le t_i, i=1,2,\ldots,N \\ \Delta P_{\mathrm{W0}}h_{\mathrm{step}}'\left(t-t_0\right)+\sum_{j=1}^{N}\left(K_{P\text{-}t}^{j}h_{\mathrm{ramp}}'\left(t-t_{j-1}\right)-K_{P\text{-}t}^{j}h_{\mathrm{ramp}}'\left(t-t_j\right)\right) \\ \quad t>t_N \end{cases} \tag{21}$$

$$\begin{cases} h_{\mathrm{step}}'(t)=r\alpha\mathrm{e}^{-\xi\Omega_{\mathrm{n}}t}\left(-\xi\Omega_{\mathrm{n}}\sin\left(\Omega_{\mathrm{r}}t+\phi\right)+\Omega_{\mathrm{r}}\cos\left(\Omega_{\mathrm{r}}t+\phi\right)\right) \\ h_{\mathrm{ramp}}'(t)=r\left(1+\alpha\mathrm{e}^{-\xi\Omega_{\mathrm{n}}t}\sin\left(\Omega_{\mathrm{r}}t+\phi\right)\right)=h_{\mathrm{step}}(t) \end{cases} \tag{22}$$

Due to the complex form of $\Delta f_{\mathrm{W}}'(t)$, it is difficult to solve

the peaking moment $t_{\mathrm{W}}^{\mathrm{peak}}$ directly. Thus, this subsection illustrates the relationship between $t_{\mathrm{W}}^{\mathrm{peak}}$ and $t_{\mathrm{L}}^{\mathrm{nadir}}$ by discussing the sign of $\Delta f_{\mathrm{W}}'(t)$ at $t_{\mathrm{L}}^{\mathrm{nadir}}$. According to the relationship between t_i and $t_{\mathrm{L}}^{\mathrm{nadir}}$, the following two conditions are discussed.

1) $t_{i-1} < t_{\mathrm{L}}^{\mathrm{nadir}} \le t_i$

$$\Delta f_{\mathrm{W}}'\left(t_{\mathrm{L}}^{\mathrm{nadir}}\right) = \sum_{j=1}^{i-1} K_{P\text{-}t}^{j}\left(h_{\mathrm{step}}\left(t_{\mathrm{L}}^{\mathrm{nadir}} - t_{j-1}\right) - h_{\mathrm{step}}\left(t_{\mathrm{L}}^{\mathrm{nadir}} - t_j\right)\right) + K_{P\text{-}t}^{i} h_{\mathrm{step}}\left(t_{\mathrm{L}}^{\mathrm{nadir}} - t_{i-1}\right) \tag{23}$$

Since $h_{\mathrm{step}}(t)$ is an incremental function and is positive within the range of $\left(t_0, t_{\mathrm{L}}^{\mathrm{nadir}}\right)$, and $K_{P\text{-}t}^{i} < 0$, $\Delta f_{\mathrm{W}}'\left(t_{\mathrm{L}}^{\mathrm{nadir}}\right) < 0$.

2) $t_{\mathrm{L}}^{\mathrm{nadir}} > t_{\mathrm{N}}$

$$\Delta f_{\mathrm{W}}'\left(t_{\mathrm{L}}^{\mathrm{nadir}}\right) = \sum_{j=1}^{N} K_{P\text{-}t}^{j}\left(h_{\mathrm{step}}\left(t_{\mathrm{L}}^{\mathrm{nadir}} - t_{j-1}\right) - h_{\mathrm{step}}\left(t_{\mathrm{L}}^{\mathrm{nadir}} - t_j\right)\right) \tag{24}$$

Since $h_{\mathrm{step}}(t)$ is monotonically increasing within $\left(t_0, t_{\mathrm{L}}^{\mathrm{nadir}}\right)$, and $K_{P\text{-}t}^{i} < 0$, $\Delta f_{\mathrm{W}}'\left(t_{\mathrm{L}}^{\mathrm{nadir}}\right) < 0$.

Combining (23) and (24), it is shown that $\Delta f_{\mathrm{W}}'\left(t_{\mathrm{L}}^{\mathrm{nadir}}\right)$ is always negative for the arbitrary parameter of the simplified TLIC power. Moreover, the frequency response model shown in Fig. 3 is a second-order underdamped system ($\xi = 0.7484 < 1$ [26]), so the frequency tends to decay under the decreasing TLIC power. It can be referred that $\Delta f_{\mathrm{W}}(t)$ has at least one extreme point within $\left(t_0, t_{\mathrm{L}}^{\mathrm{nadir}}\right)$ and the first extreme point is the maximum point, so

$$t_{\mathrm{W}}^{\mathrm{peak}} < t_{\mathrm{L}}^{\mathrm{nadir}} \tag{25}$$

In summary, the peak of the FRC under the TLIC power always occurs earlier than the nadir of the FRC corresponding to the step load, and the compensation of TLIC power for the FN is not optimal. For the following validation and calculation, the two-segment form is selected to represent the TLIC power.

C. Validation on Relationship Between Extreme Point Time

On the basis of Section III-B, for the two-segment form of the TLIC power, this subsection obtains the time $\Delta t_{\mathrm{W}}^{\mathrm{peak}}$ that is required to reach the maximum point of the FRC with different values of $K_{P\text{-}t}^{1}$. The relationship between $\Delta t_{\mathrm{W}}^{\mathrm{peak}}$ and $K_{P\text{-}t}^{1}$ is shown in Fig. 6. It can be observed that $\Delta t_{\mathrm{W}}^{\mathrm{peak}}$ is always less than $\Delta t_{\mathrm{L}}^{\mathrm{nadir}}$ and converges to $\Delta t_{\mathrm{L}}^{\mathrm{nadir}}$ as $K_{P\text{-}t}^{1}$ increases.

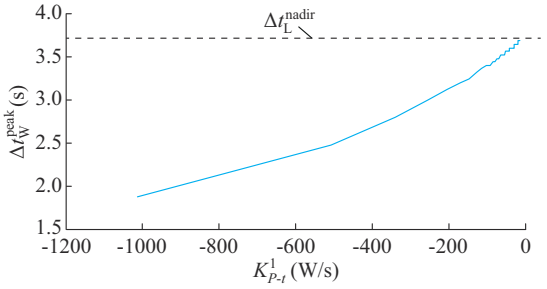

Fig. 6. $\Delta t_{\mathrm{W}}^{\mathrm{peak}}$ of frequency response under simplified wind power.

When the actual TLIC power is used as the input, the FRCs under different power are shown in Fig. 7 and $t_{\mathrm{W}}^{\mathrm{peak}} < t_{\mathrm{L}}^{\mathrm{nadir}}$. For the TLIC method, although the gentle reduction of the electrical power of WTs avoids the SFD, its non-step power form makes the maximum effect of the compensation for FN appear earlier. This lays a foundation for the mechanism analysis of the improved TLIC method based on delayed support in Section IV.

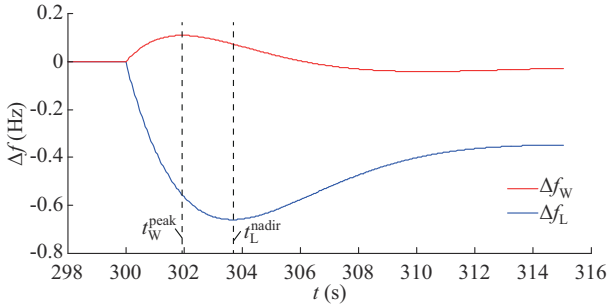

Fig. 7. FRCs under different power.

IV. Improved TLIC Method Based on Delayed Support

As shown in Fig. 8, an improved idea is proposed that the maximum point of the FRC under the TLIC power should occur simultaneously with the nadir of the FRC under the step load surge, namely $t_{\mathrm{L}}^{\mathrm{nadir}} = t_{\mathrm{W}}^{\mathrm{peak}}$, so that the FN can be compensated to the most extent. On the basis, the improved TLIC method based on delayed support is proposed.

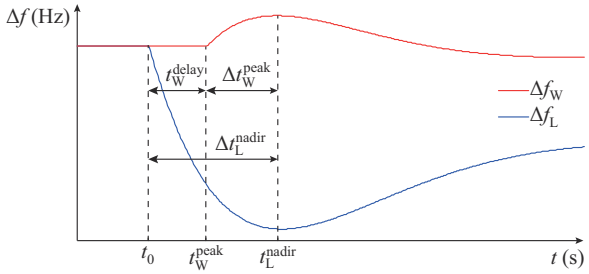

Fig. 8. Illustration of improved idea.

A. Estimation of Start Time of TLIC Method

To implement the improved idea above, the key is to determine the start time of the TLIC method (delay time $t_{\mathrm{W}}^{\mathrm{delay}}$). It can be observed from Fig. 8 that $t_{\mathrm{W}}^{\mathrm{delay}}$ is obtained by (26).

$$t_{\mathrm{W}}^{\mathrm{delay}} = \Delta t_{\mathrm{L}}^{\mathrm{nadir}} - \Delta t_{\mathrm{W}}^{\mathrm{peak}} \tag{26}$$

According to (20), $\Delta t_{\mathrm{L}}^{\mathrm{nadir}}$ is a constant value only relevant to the system parameters, so the calculation of $t_{\mathrm{W}}^{\mathrm{delay}}$ can be transformed to the calculation of $\Delta t_{\mathrm{W}}^{\mathrm{peak}}$ under the TLIC power. Hence, $\Delta t_{\mathrm{W}}^{\mathrm{peak}}$ can be estimated based on the simplified TLIC power. In this subsection, $K_{P\text{-}t}^{1}$ is set as the product of $\mathrm{d}P_{\mathrm{e}}/\mathrm{d}\omega$ and $\mathrm{d}\omega/\mathrm{d}t$ at the time of t_0 [9], [12].

$$K_{P\text{-}t}^{1} = \left.\frac{\mathrm{d}P_{\mathrm{e}}}{\mathrm{d}\omega}\frac{\mathrm{d}\omega}{\mathrm{d}t}\right|_{t=t_0} \tag{27}$$

where $\mathrm{d}P_{\mathrm{e}}/\mathrm{d}\omega$ is $K_{P\text{-}\omega}$ in (8); and $\mathrm{d}\omega/\mathrm{d}t$ is the speed acceleration of the rotor. According to the equation of motion, $\mathrm{d}\omega/\mathrm{d}t$ can be calculated.

$$J_{\mathrm{t}}\omega_0\dot{\omega}_0 = P_{\mathrm{m0}} - \left(P_{\mathrm{W0}} + \Delta P_{\mathrm{W0}}\right) \tag{28}$$

$$\left.\frac{\mathrm{d}\omega}{\mathrm{d}t}\right|_{t=t_0}=-\frac{\Delta P_{\mathrm{W0}}}{J_{\mathrm{t}}\omega_0} \tag{29}$$

where P_{m0} is the initial aerodynamic power of WT.

After the TLIC method is activated, the FRC of the TLIC power increases gradually and reaches the maximum value after $\Delta t_{\mathrm{W}}^{\mathrm{peak}}$ when the derivative of the FRC is zero. Hence, only one extreme point occurs within $\left(0,\ \Delta t_{\mathrm{W}}^{\mathrm{peak}}+\varepsilon\right)$ (ε is a positive value greater than zero), which means that $\Delta f_{\mathrm{W}}'(t)=0$ has only one solution in this range, as shown in Fig. 9. Based on the feature, the Newton-Raphson method is utilized to numerically solve $\Delta t_{\mathrm{W}}^{\mathrm{peak}}$ with the initial value set as zero. Once the solution is obtained, the solving process stops. Then, according to (26), the delay time for starting the TLIC method is estimated. From Section III and (26), it can be observed that the delay time is related to the parameters of the power system and the operation conditions of the WT (e. g., the rotor inertia, wind speed, and initial rotor speed) and the parameters of the TLIC method, and is irrelevant to the load surge. The accuracy of delay time estimation will be validated in Section V.

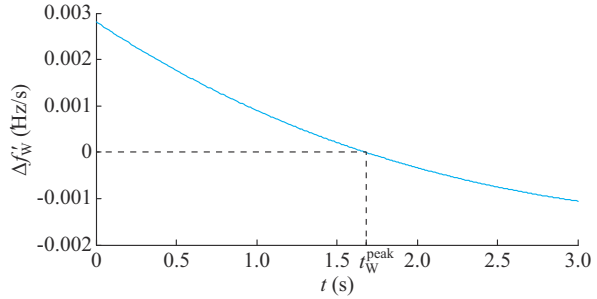

Fig. 9. Change rate of frequency under TLIC power.

B. Improved TLIC Method

Based on the estimated delay time, the improved TLIC method based on delayed support is proposed. Through matching the peaking time of the FRC under the TLIC power and the nadir time of the FRC under the load, the FN is raised to the most extent. The schematic diagram of the proposed method is shown in Fig. 10, including the following four modules.

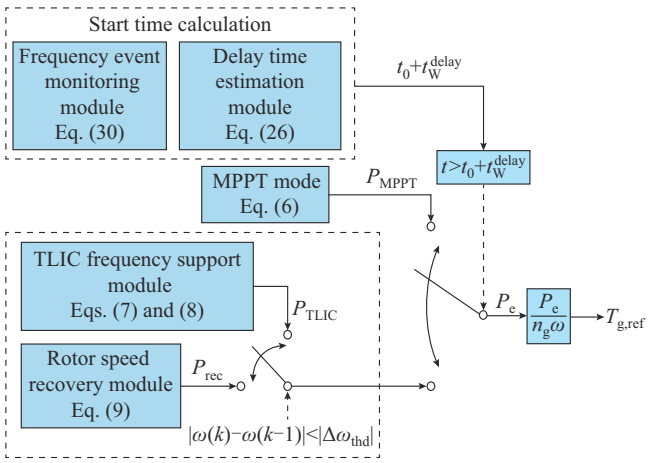

Fig. 10. Schematic diagram of proposed method.

1) Frequency event monitoring module. When the frequency deviation is beyond the threshold $\left|\Delta f_{\mathrm{thd}}\right|$, it is believed that a frequency event such as load surge or generator trip occurs, and the moment of occurrence is recorded as t_{thd}. The threshold is usually set to be 0.02 Hz [28]. Since the threshold is small, t_{thd} is approximated as t_0.

$$\left|\Delta f(t)\right|>\left|\Delta f_{\mathrm{thd}}\right| \tag{30}$$

2) Delay time estimation module. According to the estimation of $\Delta t_{\mathrm{W}}^{\mathrm{peak}}$ based on the Newton-Raphson method and (26), the delay time of starting TLIC is estimated. The start time of the TLIC method is $t_0+\Delta t_{\mathrm{W}}^{\mathrm{delay}}$.

3) TLIC frequency support module. At $t_0+\Delta t_{\mathrm{W}}^{\mathrm{delay}}$, the TLIC method is activated and the electrical power command of the WT is set according to (7) and (8).

4) Rotor speed recovery module. When the WT operates at the stable equilibrium point (point C in Fig. 2), the rotor speed is restored to the initial speed ω_0 by slightly reducing the electrical power. Specifically, when the change of rotor speed between the adjacent sampling time is less than $\left|\Delta\omega_{\mathrm{thd}}\right|$, as shown in (31), it is determined that the rotor speed has converged to ω_{C}. After that, the electrical power is reduced to P_{rec}, as shown by (6) and (9).

$$\left|\omega(k)-\omega(k-1)\right|<\left|\Delta\omega_{\mathrm{thd}}\right| \tag{31}$$

V. Experimental Validation

Based on the test bench of wind-integrated power system, the effectiveness of the proposed method is validated by a series of experiments.

A. Test Bench of Wind-integrated Power System

As shown in Fig. 11, the test bench of the wind-integrated power system [29] - [32] mainly contains the wind turbine simulator (WTS), synchronous generator simulator (SGS), and feedback load (FL). The main parameters of the test bench are given in Table I. Because of the decoupling control of the active and reactive power, the impact of the active power on the frequency is mainly focused on, and the reactive power and voltage control are not discussed. The system voltage is controlled at the value of 400 V by the excitation voltage regulator in the SGS.

1) WTS. With the algorithms of power scaling, aero-elastic coupling simulation, inertia compensation, and damping compensation, the aerodynamic and slow dynamic characteristics of real WTs with large capacity and inertia are imitated by the WTS with small capacity and low inertia. The RSC controller receives the electrical torque reference $T_{\mathrm{g,ref}}$ calculated by the PFC algorithm of the WT, so the generator output is controlled to provide the frequency support.

2) SGS. By using the algorithms of inertia compensation, prime motor, and governor simulation, the SGS can simulate the mechanical dynamic and frequency response characteristics of the real SG. The prime motor and governor simulation algorithms obtain the mechanical torque $T_{\mathrm{M,ref}}$ according to the frequency, and send it to the converter controller to control the output of the prime motor. Thus, the PFC of the SG is realized.

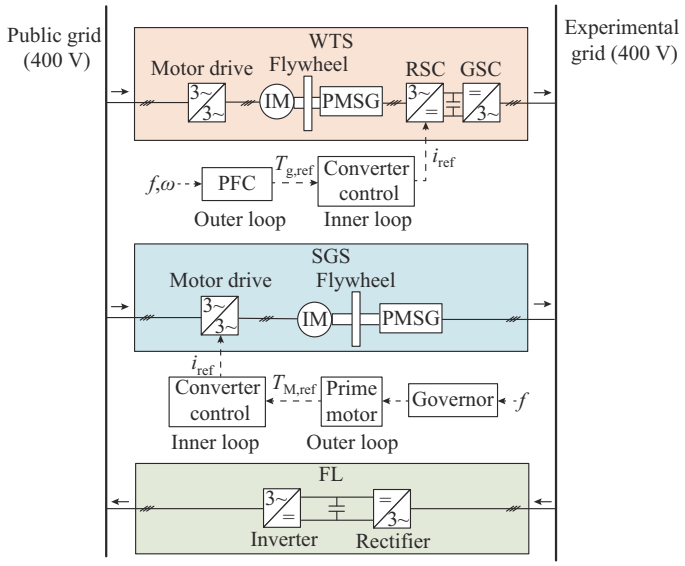

(a)

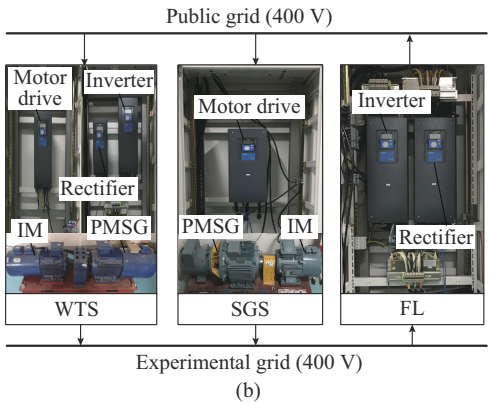

(b)

Fig. 11. Test bench of wind-integrated power system. (a) Structural diagram. (b) Physical diagram.

TABLE I
MAIN PARAMETERS OF TEST BENCH

Unit	Parameter	Value
WTS	Rated power (kW)	15
SGS	Rated power (kW)	25
	Inertial time constant (s)	5.96
	Rated speed (r/min)	1800
FL	Rated power (kVA)	37

3) FL. As the load of the experimental grid, the FL can be used to simulate the characteristics of the load. The rectifier consumes the electrical power from the experimental grid, and the inverter feeds the electrical power back to the public grid.

The simulation algorithms of WTS, SGS, and FL and the PFC algorithms are implemented in the programmable logic controller (PLC).

B. Case Study

This subsection validates the estimation accuracy of the delay time t_W^{delay} and the effectiveness of the proposed method. In order to make the experimental results more convincing, the experiment cases are carried out in several scenarios with different wind speeds, load disturbances, and wind power penetrations.

1) Validation of Estimation Accuracy of t_W^{delay}

In order to validate the estimation accuracy, the delay time obtained by the proposed method is first compared with the optimal delay time obtained by traversal, and the FNs corresponding to the two delay time are compared. Several cases are carried out with different wind speeds (7 m/s, 8 m/s, 9 m/s, etc.), different wind power penetration rates (15%, 20%, 30%, etc.), and different load perturbations (1.2 kW, 1.5 kW, 2.0 kW, etc.). The differences between the estimated delay time and the optimal delay time are obtained, and the average of the differences is only about 0.15 s. The FNs corresponding to the two delay time are close. In the case with the wind speed of 8 m/s, the penetration rate of 30%, and the load surge of 1.2 kW, the estimated delay time, optimal delay time, and their corresponding FNs are shown in Table II and Fig. 12. It can be referred that the estimation error of delay time calculated by the proposed method is acceptable.

TABLE II
VALIDATION OF ESTIMATION ACCURACY OF DELAY TIME

Method	Delay time (s)	FN (Hz)
Proposed	2.30	–0.3970
Traversal	2.48	–0.3979

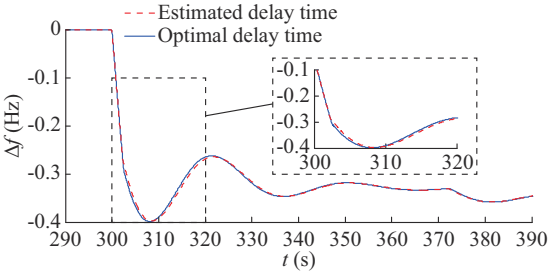

Fig. 12. Comparison of FNs with estimated and optimal delay time.

2) Comparative Analysis of Frequency Regulation Effect

To validate the effect of the proposed method on the FN, three methods are compared, including MPPT, conventional TLIC, and proposed method in two experimental cases shown in Table III. The trajectories of the frequency deviation, rotor speed, output power of WTS, and output power of SGS in two experimental cases are presented in Fig. 13 and Fig. 14, respectively.

In Case 1, when the WTS operates in MPPT mode, the power support is unavailable for the active power balance. Only the SG participates in the frequency regulation, and the FN Δf_{nadir} is –0.6344 Hz. When the WTS participates in the frequency regulation and the conventional TLIC method is triggered immediately when the load event occurs, the kinetic energy is released to support the power balance so that the nadir is raised to –0.4503 Hz.

TABLE III
PARAMETERS OF TWO EXPERIMENTAL CASES

Parameter	Case 1	Case 2
Wind speed (m/s)	8.0	10.0
Initial output power of WTS (kW)	3.6	7.1
Initial output power of SGS (kW)	8.4	4.9
Wind power penetration rate (%)	30.0	59.0
Load (kW)	12.0	12.0
Load surge (kW)	1.2	1.5

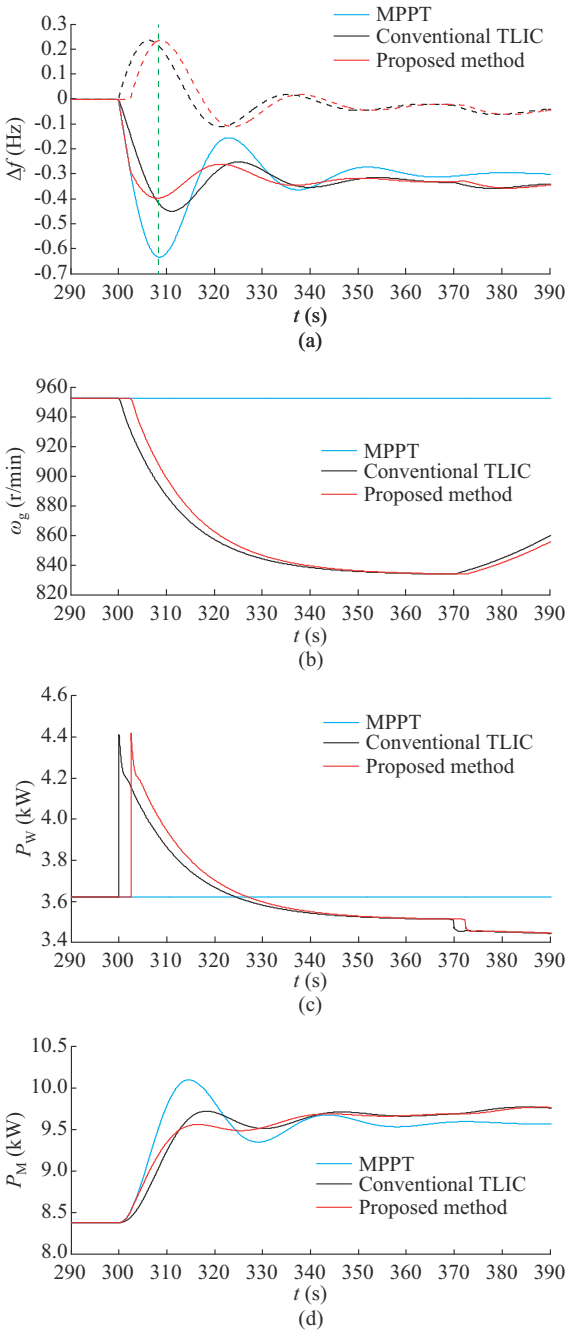

Fig. 13. Experimental results of different methods in Case 1. (a) Frequency deviation. (b) Rotor speed. (c) Output power of WTS. (d) Output power of SGS.

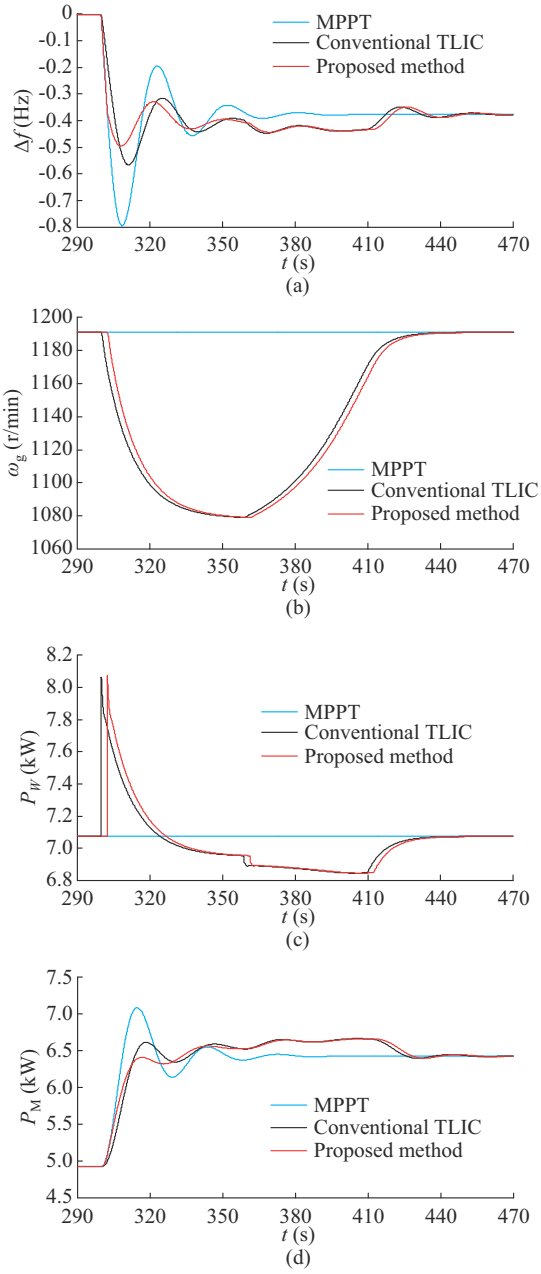

Fig. 14. Experimental results of different methods in Case 2. (a) Frequency deviation. (b) Rotor speed. (c) Output power of WTS. (d) Output power of SGS.

It is found that the peaking time of the FRC corresponding to the conventional TLIC method is always earlier than $t_{\mathrm{L}}^{\mathrm{nadir}}$, thus the maximum effect of the WTS on the FN is not exerted, as shown by the black dashed line in Fig. 13(a). By delaying the start time of the conventional TLIC method with 2.32 s, the peaking time of the FRC under the TLIC power occurs at the nadir time under the load surge, as shown by the red dashed line and the green dashed line in Fig. 13(a). The maximum effect of wind power manages to raise the FN to –0.3979 Hz.

It should be noted that the proposed method improves the FN at the cost of worsening the initial change rate of the frequency after the event, but it is at the same level as the

MPPT mode and the worse results are not caused. Moreover, it is worth pointing out that the proposed method only delays the start time of the TLIC method, rather than changing the TLIC method itself (e. g., the initial power increment ΔP_{W0} and the slope of the power-speed curve $K_{P\text{-}\omega}$), so the dynamic process of the rotor speed is not changed. After that, the WT converges to the stable equilibrium point C and then recovers the rotor speed. This means that the proposed method does not destabilize the WTS, and further enhances the FN.

In other words, the WT does not inject additional electrical power and energy, but the FN gets raised. Not only enough supportive power should be injected, but the coordination between PFCs of WTs and SGs is necessary. The FRC of the load power is essentially only the frequency regulation result of SGs, while matching the peak of the FRC under the TLIC power and the nadir under the load surge is a feasible measure to coordinate the active power output of the WT and SG. As can be observed in Fig. 13(d), the proposed method excites more output power of SGS after the frequency event compared with the conventional TLIC method.

In Case 2, as can be observed from Table IV and Fig. 14, the FN Δf_{nadir} is –0.7943 Hz without the frequency support of the WTS. When the conventional TLIC method is utilized to provide the frequency support, the FN is boosted to –0.5658 Hz. By delaying the start time of the conventional TLIC method with 2.52 s, the FN is further raised to –0.4959 Hz. Before the activation of the proposed method, the output power of the SGS is more than that under the conventional TLIC method.

TABLE IV
COMPARISON OF FREQUENCY REGULATION EFFECT INDICES

Case	Method	Δf_{nadir} (Hz)	The maximum RoCoF (Hz/s)
Case 1	MPPT	–0.6344	–0.1207
	Conventional TLIC	–0.4503	–0.0475
	Proposed method	–0.3979	–0.1207
Case 2	MPPT	–0.7943	–0.1509
	Conventional TLIC	–0.5658	–0.0585
	Proposed method	–0.4959	–0.1509

On the other hand, from the complete trajectory of the electrical power and the rotor speed of the WTS, it can be observed that the WTS succeeds in recovering to the initial operating point just by the slight electrical power drop when using the proposed method. And it has a small impact on the frequency. That is to say, the proposed method further improves the FN without affecting the stability of WTS.

VI. CONCLUSION

To retrain the fast drop of the frequency, the PFCs are mostly activated immediately once the load surge event occurs so that the kinetic energy is released to support the power balance. The FN is an important index of the PFC performance. In reality, it is found that the maximum point of the FRC excited by the PFC and the minimum point of the FRC excited by the load surge do not always occur simultaneously. That is, the maximum effect of the PFC is not exerted to boost the FN. For the TLIC method discussed in this paper, by analyzing the relationship between the maximum and minimum point time of the FRCs under the TLIC power and load power, respectively, it is inferred that the maximum point of the FRC under wind power appears earlier than the nadir corresponding to the load. Hence, the improved method that the maximum and minimum points are matched at the same time is proposed. Then, the TLIC method based on delayed support is proposed. This method further improves the FN without affecting the stability of WTs by delaying the start time of the PFC of WTs. This work can contribute to the performance improvement of the PFC in engineering applications by only regulating the start time.

REFERENCES

[1] X. Tang, F. Miao, Z. Qi *et al*., "Survey on frequency control of wind power," *Proceedings of the CSEE*, vol. 34, no. 25, pp. 4304-4314, Sept. 2014.
[2] J. Liu, W. Yao, J. Wen *et al*., "Prospect of technology for large-scale wind farm participating into power grid frequency regulation," *Power System Technology*, vol. 38, no. 3, pp. 638-646, Mar. 2014.
[3] A. Attya, J. Dominguez-Garcia, and O. Anaya-Lara, "A review on frequency support provision by wind power plants: current and future challenges," *Renewable and Sustainable Energy Reviews*, vol. 81, pp. 2071-2087, Jun. 2018.
[4] Y. Cheng, R. Azizipanah-Abarghooee, S. Azizi *et al*., "Smart frequency control in low inertia energy systems based on frequency response techniques: a review," *Applied Energy*, vol. 279, p. 115798, Sept. 2020.
[5] K. Liao, Y. Xu, M. Yin *et al*., "A virtual filter approach of wind energy conversion systems for mitigating power system frequency fluctuations," *IEEE Transactions on Sustainable Energy*, vol. 11, no. 3, pp. 1268-1277, Jul. 2020.
[6] J. Morren, J. Pierik, and W. Haan, "Inertial response of variable speed wind turbines," *Electric Power Systems Research*, vol. 76, pp. 980-987, Jul. 2006.
[7] P. Verma, S. K., and B. Dwivedi, "A cooperative approach of frequency regulation through virtual inertia control and enhancement of low voltage ride-through in DFIG-based wind farm," *Journal of Modern Power Systems and Clean Energy*, vol. 10, no. 6, pp. 1519-1530, Nov. 2022.
[8] Z. Wu, W. Gao, T. Gao *et al*., "State-of-the-art review on frequency response of wind power plants in power systems," *Journal of Modern Power Systems and Clean Energy*, vol. 6, no. 1, pp. 1-16, Jan. 2018.
[9] W. Bao, L. Ding, Z. Liu *et al*., "Analytically derived fixed termination time for stepwise inertial control of wind turbines – Part I: analytical derivation," *Journal of Electrical Power and Energy Systems*, vol. 121, p. 106120, Oct. 2020.
[10] Y. Guo, W. Bao, L. Ding *et al*., "Analytically derived fixed termination time for stepwise inertial control of wind turbines – Part II: application strategy," *Journal of Electrical Power and Energy Systems*, vol. 121, p. 106106, Oct. 2020.
[11] M. Kheshti, L. Ding, W. Bao *et al*., "Toward intelligent inertial frequency participation of wind farms for the grid frequency control," *IEEE Transactions on Industrial Informatics*, vol. 16, no. 11, pp. 6772-6786, Nov. 2020.
[12] M. Kang, K. Kim, E. Mulkadi *et al*., "Frequency control support of a doubly-fed induction generator based on the torque limit," *IEEE Transactions on Power Systems*, vol. 31, no. 6, pp. 4575-4583, Nov. 2016.
[13] D. Yang, M. Kang, J. Kim *et al*., "Stable stepwise short-term frequency support of a DFIG-based wind farm," *International Transactions of Electric Energy Systems*, vol. 28, no. 3, pp. 1-15, Mar. 2018.
[14] J. Zhao, M. Li, X. He *et al*., "Coordinated control strategy of wind power and energy storage in frequency regulation based on torque limit control," *Transactions of China Electrotechnical Society*, vol. 34, no. 23, pp. 4982-4990, Dec. 2019.
[15] E. Itani, D. Annakkage, and G. Joos, "Short-term frequency support utilizing inertial response of DFIG wind turbines," in *Proceedings of IEEE PES General Meeting*, Detroit, USA, Jul. 2011, pp. 1-8.
[16] M. Kheshti, S. Lin, X. Zhao *et al*., "Gaussian distribution-based iner-

tial control of wind turbine generators for fast frequency response in low inertia systems," *IEEE Transactions on Sustainable Energy*, vol. 13, no. 3, pp. 1641-1653, Jul. 2022.
[17] M. Kang, E. Muljadi, K. Hur *et al*., "Stable adaptive inertial control of a doubly-fed induction generator," *IEEE Transactions on Smart Grid*, vol. 7, no. 6, pp. 2971-2979, Nov. 2016.
[18] M. Kang, J. Lee, K. Hur *et al*., "Stepwise inertial control of a doubly-fed induction generator to prevent a second frequency dip," *Journal of Electrical Engineering and Technology*, vol. 10, no. 6, pp. 2221-2227, Nov. 2015.
[19] W. Gu, M. Yin, Z. Chen *et al*., "On influence of delayed support of wind power on primary frequency regulation of power systems," in *Proceedings of IEEE Sustainable Power & Energy Conference*, Nanjing, China, Dec. 2021, pp. 743-747.
[20] M. Nasiri, J. Milimonfared, and S. Fathi, "Modeling, analysis and comparison of TSR and OTC methods for MPPT and power smoothing in permanent magnet synchronous generator-based wind turbines," *Energy Conversion and Management*, vol. 86, pp. 892-900, Oct. 2014.
[21] B. Boukhezzar and H. Siguerdidjane, "Nonlinear control of a variable-speed wind turbine using a two-mass model," *IEEE Transactions on Energy Conversion*, vol. 26, no. 1, pp. 149-162, Mar. 2011.
[22] F. Liu, Z. Liu, S. Mei *et al*., "ESO-based inertia emulation and rotor speed recovery control for DFIGs," *IEEE Transactions on Energy Conversion*, vol. 32, no. 3, pp. 1209-1219, Sept. 2017.
[23] K. Liao, D. Lu, M. Wang *et al*., "A low-pass virtual filter for output power smoothing of wind energy conversion systems," *IEEE Transactions on Industrial Electronics*, vol. 69, no. 12, pp. 12874-12885, Dec. 2022.
[24] J. Merida, L. Aguilar, and J. Davila, "Analysis and synthesis of sliding mode control for large scale variable speed wind turbine for power optimization," *Renewable Energy*, vol. 71, pp. 715-728, Nov. 2014.
[25] D. Hansen, M. Altin, D. Margaris *et al*., "Analysis of the short-term overproduction capability of variable speed wind turbines," *Renewable Energy*, vol. 68, pp. 326-336, Aug. 2014.
[26] P. Anderson and M. Mirheydar, "A low-order system frequency response model," *IEEE Transactions on Power Systems*, vol. 5, no. 3, pp. 720-729, Aug. 1990.
[27] C. Richard and H. Robert, "Modern control system," in *Marquette University Faculty Book*, 13th ed., London: Pearson, 2016.
[28] M. Kang, E. Muljadi, K. Hur *et al*., "Stable adaptive inertial control of a doubly-fed induction generator," *IEEE Transactions on Smart Grid*, vol. 7, no. 6, pp. 2971-2979, Nov. 2016.
[29] M. Yin, W. Li, C. Y. Chung *et al*., "Inertia compensation scheme of WTS considering time delay for emulating large-inertia turbines," *IET Renewable Power Generation*, vol. 11, no. 4, pp. 529-538, Mar. 2017.
[30] W. Li, M. Yin, Z. Chen *et al*., "Inertia compensation scheme for wind turbine simulator based on deviation mitigation," *Journal of Modern Power System and Clean Energy*, vol. 5, no. 2, pp. 228-238, Mar. 2017.
[31] Y. Xu, M. Yin, Z. Chen *et al*., "Damping compensation strategy of wind turbine simulator and experimental verification," *Electric Power Engineering Technology*, vol. 36, no. 6, pp. 46-52, Nov. 2017.
[32] L. He, M. Yin, S. Liu *et al*., "Wind turbine simulator for aero-elastic coupling simulation," *Electric Power Engineering Technology*, vol. 37, no. 5, pp. 14-19, Sept. 2018.

Wei Gu received the B. Eng. degree in electrical power engineering from Nanjing University of Science and Technology, Nanjing, China, in 2017. He is currently pursuing the Ph. D. degree in control science and engineering with the School of Automation, Nanjing University of Science and Technology. His research interest includes active power control of wind turbines.

Zaiyu Chen received the B.S. degree in information and computing science and the Ph.D. degree in control science and engineering from Nanjing University of Science and Technology, Nanjing, China, in 2012 and 2019, respectively. He was a Research Fellow with the School of Electrical and Electronic Engineering, Nanyang Technological University, Singapore, from Jan. 2020 to Mar. 2021. He is currently a Lecturer with the School of Automation, Nanjing University of Science and Technology. His research interests include active power control of wind turbines and its application in power system frequency regulation.

Qun Li received the B.Eng. degree in electronic equipment structure design from Southeast University, Nanjing, China, in 1989, the M. Eng. degree in electronic equipment structure design from Xidian University, Xi'an, China, in 1995, and the Ph.D. degree in power systems and automation from Southeast University, in 1999, respectively. He is currently a Professorate Senior Engineer with the State Grid Jiangsu Electric Power Co., Ltd. Research Institute, Nanjing, China. His research interests include power quality analysis and renewable power integration.

Minghui Yin received the B. Eng. and M. Eng. degrees in electrical power engineering and the Ph. D. degree in control science and engineering from Nanjing University of Science and Technology, Nanjing, China, in 1999, 2002, and 2009, respectively. He was a Research Assistant with the Department of Electrical Engineering, the Hong Kong Polytechnic University, Hong Kong, China, from Jul. 2007 to Jul. 2008. From Jan. 2016 to Jan. 2017, he was a Visiting Scholar with the School of Electrical and Information Engineering, the University of Sydney, Sydney, Australia. He is currently a Professor with the School of Automation, Nanjing University of Science and Technology. His major research interests include wind power conversion system and power system transient stability.

Qiang Li received the B.Eng., M.Eng., and Ph.D. degrees in power systems and automation from Hohai University, Nanjing, China, in 2003, 2006, and 2011, respectively. He is currently a Professorate Senior Engineer with the State Grid Jiangsu Electric Power Co., Ltd. Research Institute, Nanjing, China. His research interests include flexible transmission of mid-far sea wind power.

Yun Zou received the B.S. degree in mathematics from Northwestern University, Xi'an, China, in 1983, and the M. S. and Ph. D. degrees in control theory and control engineering from Nanjing University of Science and Technology, Nanjing, China, in 1987 and 1990, respectively. He is currently a Professor with the School of Automation, Nanjing University of Science and Technology. His current research interests include differential-algebraic equation systems, two-dimensional systems, singular perturbations, and transient stability of power systems and electricity market.